

Assessing the Evolution of the Solar Wind through the Spectrum
of Velocity Fluctuations from 1 – 5 AU.

Austin Atkins
Department of Physics
University of New Hampshire
Durham, NH 03824

5/16/2013

Abstract:

Turbulent processes occur in the solar wind and contribute to solar wind evolution and heating. Measurements of the spectrum of velocity and magnetic field fluctuations agree well with predictions of Kolmogorov turbulence theory for energy cascade near 1 AU. Recent studies show that the power laws of the magnetic field fluctuations in the inertial range diverge from the power laws of velocity fluctuations. We analyze the velocity spectra of the solar wind by extracting intervals from Voyager II data between 1 and 5 AU. Using Fast Fourier Transforms we compare the slopes of the velocity spectra to the $-5/3$ value predicted by the Kolmogorov model and the $-3/2$ slope obtained by previous studies. We observe how the slope changes with radial distance. This work remains in progress and we find little correlation between slopes of spectra predicted by Kolmogorov theory and analysis of previous studies. We suspect the accuracy of the Voyager II data and begin surveying the solar wind spectra from Voyager I data.

Acknowledgements:

I would like to thank Charles Smith for the wealth of opportunities he's provided me over the past year. His dedication to research, his students and their success is self evident. I would also like to thank Bernard Vasquez for the many occasions of willingness to help on short notice and the endless programming assistance he's provided.

Contents

1. The Solar Wind	
1.1 Early Remote Observations.	5
1.2 Parker Predictions.	5
1.3 Basics of the Solar Wind	7
1.4 Coronal Mass Ejections	9
1.5 Shocks	11
1.6 Corotating Interacting Regions	12
2. Magnetohydrodynamics	
2.1 Background of MHD	13
2.2 Equations of MHD	13
2.3 Alfven Waves	14
3. Turbulence	
3.1 Elements of Turbulence	18
3.2 The Navier-Stokes Equation	18
3.3 Kolmogorov Theory	20
4. The Spectrum of Velocity Fluctuations	
4.1 Motivation	22
4.2 Overview	22
4.3 Data Preprocessing	22
4.4 Velocity Spectra	23
4.5 Interval Modification	24
4.6 Summary	25

Chapter 1

The Solar Wind

1.1 Early Remote Observations

The earliest observations of the sun by the unaided eye date earlier than 5000 BC during solar eclipses. The fortunate similarity of the angular diameter of the moon and sun makes visible the corona by blocking most of sun's radiance. Observations of the sun by the aided eye date to the early 17th century not long after the invention of the telescope. The observations of the planets and sun conflicted with the geocentric view of the solar system and encouraged the advancement of telescopes and astronomical observational techniques. Many, particularly Galileo and Newton, risked eye damage by direct observation until the method of projecting the sun's image onto a screen was implemented [1]. The first sightings of sunspots are recorded in ancient drawings and texts, many by Chinese astronomers from sightings with the naked eye. The introduction of the telescope in 1608 allowed detailed drawings of solar spots and began the first systematic study of solar irregularities and the establishment of consistent data analysis to predict astronomical events.

The second half of 17th century observations revealed significant variation in the number of observable sunspots and later analysis showed that sunspot regularity activity occurred roughly every 11 years [2]. Solar studies gained popularity after the publication of "Solar Observations during 1843" by Heinrich Schwabe and more sophisticated observations were made with the invention of the spectrometer and later the spectroheliograph. In 1859, British astronomer Richard Carrington observed two regions of intense light while studying sunspots from a projected image that faded after five minutes. Less than 18 hours after the event a geomagnetic storm occurred and increased activity of the Aurora and telegraph interference were observed [2].

Early studies indicated a relationship between solar activity and atmospheric influence that left some interactions unexplainable until halfway through the 20th century. Geomagnetic disturbances were linked with solar activity but the mechanisms creating solar storms were widely misunderstood until a significant advancement was made by George Hale in 1908. Atop a 60 foot tower using a modified spectrohelioscope he discovered a shift in the hydrogen-alpha series via the Zeeman effect [3]. Spectroscopic analysis performed by Bengt Edlen in 1942 showed previously unknown spectral lines from the solar corona that would result from extremely high temperatures [4]. The million degree corona extends a significant distance into space and began the accelerated investigation of the solar wind at the start of the space age.

1.2 Parker Predictions

Early observations indicating that matter is emitted by the sun came from comets' tails directed radially away from the sun. Early theories considered radiation pressure to be the cause of the

outward flowing comet tails but photon pressure proves insufficient for the extent to which the tails depart. A steady outflow of particles from the sun was the most likely source of the interaction. The model that interplanetary space was relatively void of matter was popular, even more so among the public [5]. The developing model of an ionized plasma breeze leaving the sun was greatly strengthened by Parker's 1958 publication showing that the breeze could travel at supersonic speeds. His paper encountered strong opposition and experimental justification came in 1959 with the Soviet satellite Luna 1 and subsequent observations verified the predictions [2].

Previous models of the solar corona existing in hydrostatic equilibrium were insufficient in explaining a solar breeze and motivated Parker to consider the corona from a hydrodynamic perspective. Parker modeled the solar atmosphere as a quasi-neutral fluid with only radial variations. Considering a region of an ideal fluid, using an isothermal approximation and implementing Bernoulli's equation Parker arrived at the following equation

$$\frac{1}{u} \frac{du}{dr} \left(\frac{u^2}{v_s^2} - 1 \right) = \frac{2}{r} \left(1 - \frac{r_c}{r} \right) \quad (1)$$

where u is the velocity, r is the radius, v_s is the isothermal sound speed and $r_c = M_\odot G / 2V_s^2$. Equation 1 can be solved for the velocity of the expansion of the isothermal model as a function of radial distance [5]. Observation of the differential equation reveals that several solutions are permitted with interesting consequences determined by the rate at which the left and right hand sides vanish. The various classes of solutions are shown in Figure 3.

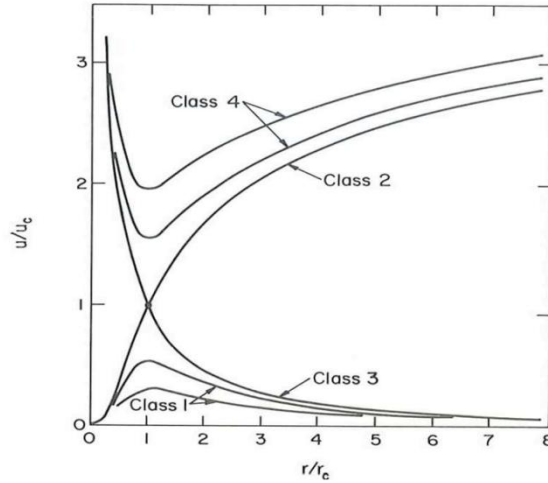


Figure 1: The various solutions of Eq. 1 are plotted versus radial distance [6].

Noting the intersection of the Class 2 and Class 3 solutions, Figure 1 demonstrates the radial distance at which the flow becomes supersonic. It is evident that several solutions are unphysical. For Class 4 solutions at small radial values the flow begins supersonic and evidence doesn't support this prediction. The Class 3 solution likewise begins supersonic then drops to subsonic with increasing distance. Interesting solutions from Class 1 predict that the flow from the corona, by the model, begins subsonic, peaks when $r = r_c$ and decreases monotonically with increasing distance. Parker's success with the hydrodynamic approach to the corona is visible

with the Class 2 solution. The flow begins subsonic, becomes supersonic at the critical radius and increases in velocity for two orders of r/r_c with increasing radial distance. The model shows that a supersonic flow from the sun is possible. Many were skeptical of the predictions until satellite data verified the wind.

A simplified model of the solar wind origin is constructed from a kinetic description of the sun's corona. Consider the scaling of the solar atmosphere by noting that the temperature, pressure and density decrease with radial distance away from the sun. Consider a box in this region. Collisions of coronal gas result in a pressure differential on the box with greater pressure closer to the sun due to higher particle densities and temperatures. If this pressure differential produces an outward force greater than the gravitational attraction, the region will be accelerated away from the sun [6]. In Parker's 1958 publication the only known mechanism that could account for the solar wind required the million degree temperature of the corona, though the mechanism responsible for this heating was unknown and is still under intense research today.

A second prediction of Parker's 1958 publication is the effect of the sun's magnetic field with the angular velocity included. The effect is enhanced by the conductivity of the solar wind, introduced in section 2.3, and we mention only the results of the prediction here. The trajectory of charged particles is influenced by magnetic fields, likewise, magnetic fields are influenced by the motion of charged particles. The sun's magnetic field can be naively considered that of a dipole that is largely modified by the presence of the solar wind and the sun's angular velocity. The sun's magnetic field structure is preserved in the conducting solar wind and the radial component of the flow draws the magnetic field lines outward [8]. A sketch of the field approximation is shown in Figure 2.

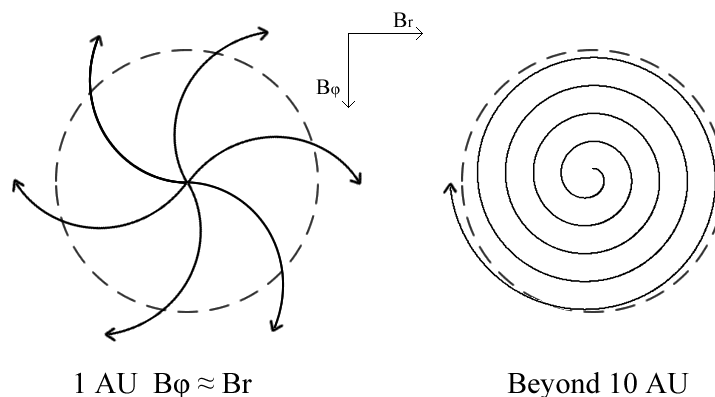


Figure 2: Parker spirals at 1 and 10 AU. At earth, the magnetic field is approximately 45 degrees.

The finite propagation of magnetic field information results in the Archimedes spiral of the sun's magnetic field. This effect is enhanced by the solar wind that preserves the magnetic field by freezing the magnetic flux.

1.3 Basics of the solar wind

The temperature of the sun's corona exceeds $10^6 K$ thus the solar atmosphere is entirely ionized. The thermal velocity of the electrons is greater than the thermal velocity of the protons thus the electrons are further away in the corona. This establishes an electric field directed radially

outward that further accelerate the protons that produce the solar wind. This supersonic flow composes the heliosphere and has been studied by a wealth of satellites between .3 and 100 AU over the past four decades. Most of the flow consists of protons and electrons with approximately a 4% abundance of ionized helium and trace amounts of heavier elements. The basic properties of the solar wind at 1 AU are listed in Table 1.

Parameter	Fast wind	Slow wind
Velocity (kms^{-1})	750	400
p^+ density (m^{-3})	$2.5 \cdot 10^6$	$10 \cdot 10^6$
e^- density (m^{-3})	$4 \cdot 10^6$	$12 \cdot 10^6$
Temperature (K)	$2 \cdot 10^5$	$4 \cdot 10^4$

Table 1: Basic properties of the solar wind at 1 AU [5].

The fast solar wind arises from open field lines around the north and south poles of the sun where the magnetic field is radially outward. The slow wind arises from closed field lines near the equator. During solar minimum, the fast wind varies little except for regions near the equator. During solar maximum the fast and slow wind velocity distributions vary significantly as solar behavior becomes more chaotic [5]. The solar wind proton and electron densities are approximately equal and compose a nearly collisionless plasma. This outward flow drags the sun's magnetic field outward from the sun. In the reference frame of the earth, the approaching magnetic field gives rise to an electric field that drives currents at the earth's magnetosphere that lead to the Aurora [6].

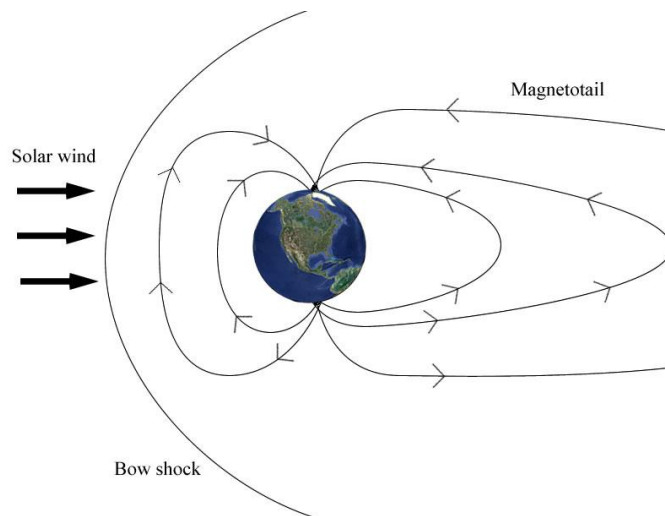


Figure 3: Solar wind stretches the magnetosphere to a long tail where magnetic reconnection occurs. The earth's magnetic field is compressed on the day side and produces the bow shock. Charged particles are steered towards the poles

The solar wind compresses the earth's magnetic field on the day side and stretches the earth's magnetic field on the night side as depicted in Figure 3. The day side of the earth's magnetic field deflects the solar wind forming the bow shock that varies in radial distance from the earth in response to increased solar activity.

1.4 Coronal Mass Ejections

The sun's rotational period at the equator is approximately 25 days long and decreases as latitude increases [5]. The varying density of the sun coupled with the differential rotation of plasma establishes a complex dynamo effect that produces yet unpredictable magnetic storms on the sun. Changes in temperature, density, conductivity, and velocity contribute to the complexity of the magnetic behavior on the sun and its 11 year cycle of magnetic polarity inversion. During solar maximum, significant variations occur in solar wind velocity spectra, solar flare occurrences and sunspots. A solar flare is observed as a sudden localized increase in brightness on the sun where charged particles are tied to looping magnetic field lines [5]. This releases energy via magnetic reconnection as the magnetic topology quickly rearranges converting magnetic field energy into kinetic and thermal energy [9]. Since early studies of solar storms in the 19th century were recorded, large disturbances to the earth's geomagnetic environment were attributed to solar flares but are now linked to larger events called Coronal Mass Ejections (CME).

Solar flares and CME's often occur within short time intervals of each other but are causally unrelated. During a CME, intense outbursts of charged particles are channeled by magnetic fields and travel up to $4,000 \text{ kms}^{-1}$ [9].

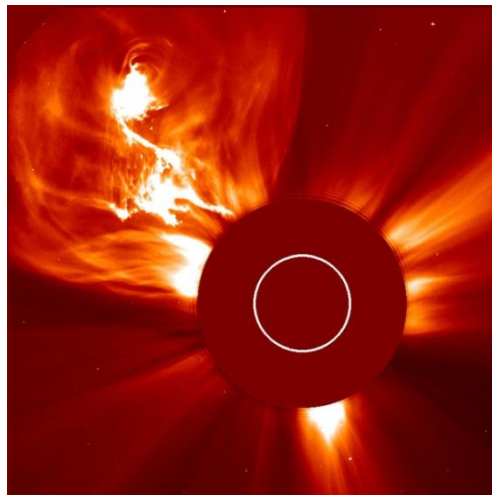


Figure 4: A CME coronagraph taken by the Solar and Heliospheric Observatory (SOHO) on January 4, 2002 [10].

There are approximately three CME's per day during solar maximum and one per five days during solar minimum [9]. The mass of charged particles emitted disturbs the interplanetary environment and upon reaching the earth interacts with the magnetosphere. The charged particles are directed by the magnetic field lines towards the poles where they interact with the ionosphere producing geomagnetic storms. Their influence ranges from satellite and radio interference to induced currents in electrical transmission lines disabling power grids. Figure 5

provides a comparison of Advanced Composition Explorer (ACE) data from solar minimum and solar maximum. The right half of Figure 5 shows a week of relatively minor fluctuations compared to that in 2000. The magnitude of the magnetic field on the left side of Figure 5 varies by nearly 20 nT with rapid transitions. The significant variability is evident in most of the measured parameters of the two CME's where the plots of 2004 are noticeably less variable. The high speed CME matter plows into the solar wind giving rise to rapid changes in particle density, temperature and velocity called a shock covered in Section 1.5.

The mass of CME's is predicted with large uncertainties by analyzing coronagraphs similar to of Figure 1. Measuring the intensity of the emission, the plasma density is approximated by the physics of Thompson scattering. The difficulty with this approach and similar techniques in the X-ray or extreme ultraviolet range are limitations of the two dimensional analysis [9]. Measurements from multiple craft help elude this approximation.

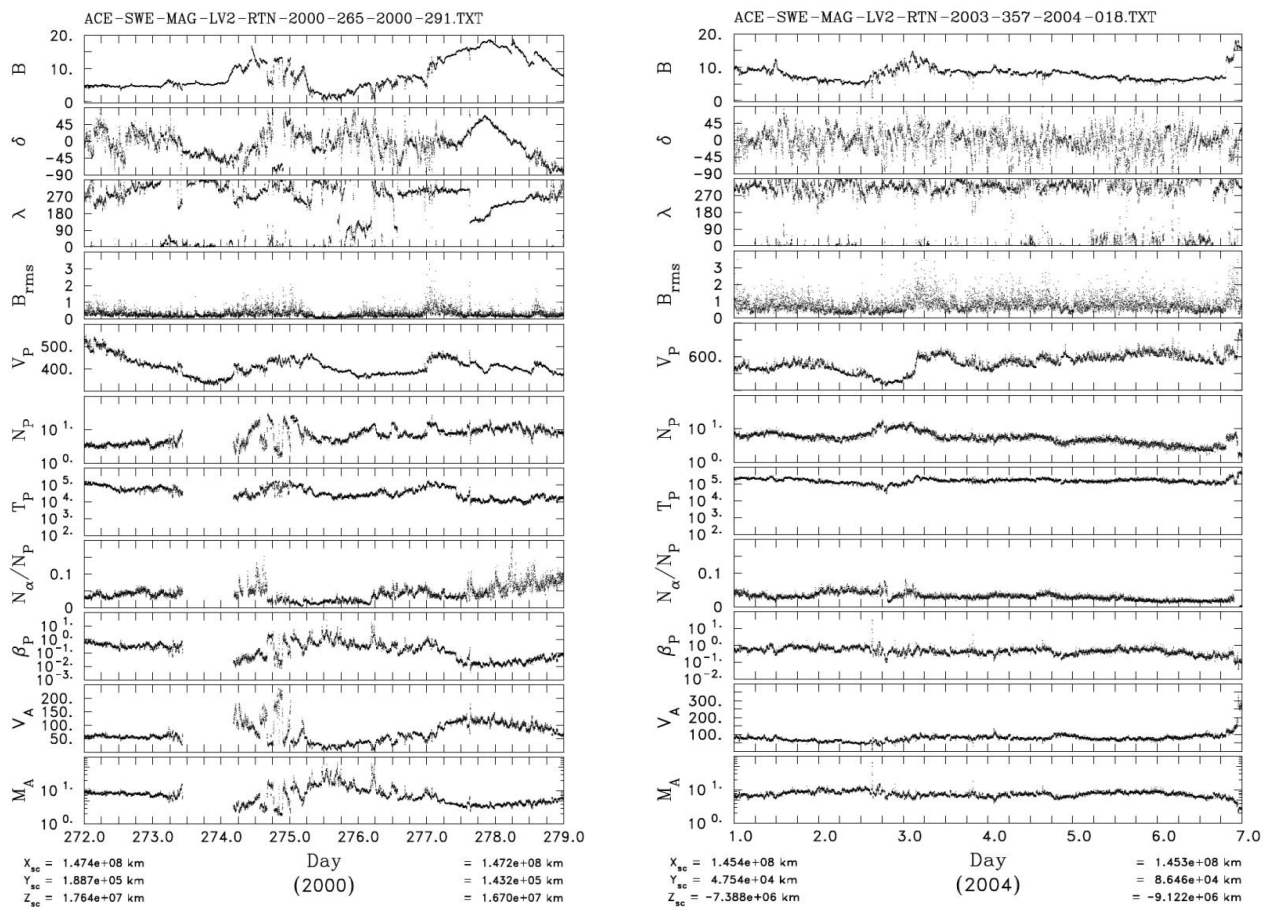


Figure 5: ACE data from 2000 and 2004. All magnetic fields in nT , density in cm^{-3} , velocity in kms^{-1} , angles in degrees. Data is represented in a Radial Tangential Normal (RTN) coordinate system. Labels, from top to bottom are: magnitude of magnetic field, magnetic latitude, magnetic longitude, rms magnetic vector, wind speed, proton density, proton temperature (K), alpha particle density, proton plasma beta, Alfven speed, Mach number. The left plot shows two CME events during solar maximum compared to conditions of solar minimum of the right plot. The two events appear after day 274 and day 277 [11].

1.5 Shocks

The velocity of a CME can quadruple the velocity of the fast solar wind. The interaction of the two masses results in abrupt increases in particle density, temperature, magnetic field strength, and velocity. The behavior of shocks is exemplified by considering an interaction in air less than the speed of sound. When an object is placed in motion in a fluid, sound waves provide a means for the fluid to adapt to compressions. The motion transfers information to the undisturbed medium ahead and the air can move out of the way. With movement exceeding the speed of sound, information cannot propagate ahead leaving the medium unperturbed. With a compressed region immediately in front of the object and an uncompressed region ahead, two regions exist with different sound speeds due to the different density and temperature. The supersonic information just ahead of the object encounters a subsonic medium that doesn't readily move. This interaction is called a shock and the information from the shock propagates opposite the direction of the object at supersonic speeds [5].

This fluid model is inappropriate to the solar wind where mean free paths are on the order of 1 AU. The collisionless plasma is given sufficient communication via the electromagnetic interaction. Shocks occur frequently in the solar wind when a fast wind overruns a slow wind and provides a mark between mediums. CME's develop strong shocks with large velocity differences from both the fast and slow wind. Evidence of a shock is shown in Figure 6.

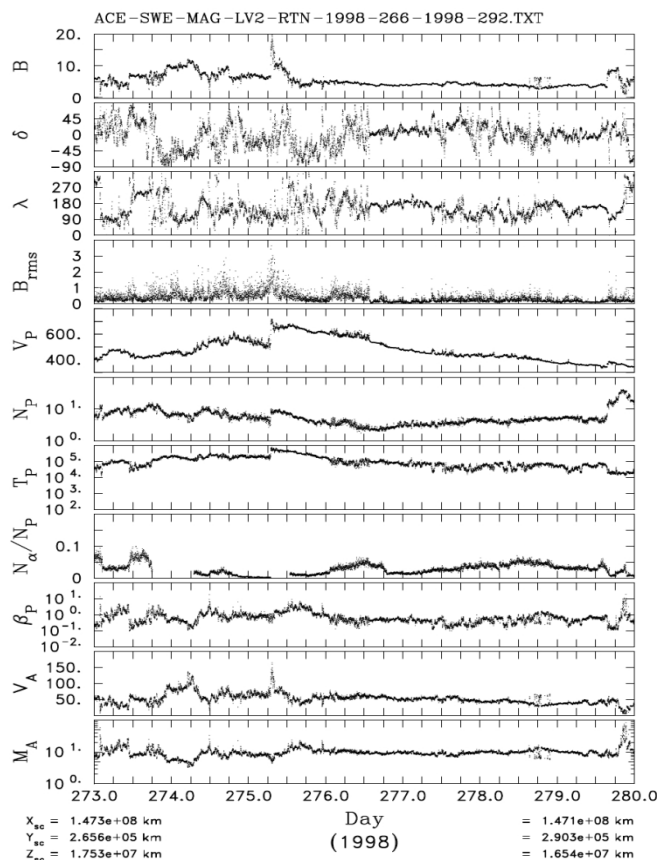


Figure 6: A shock from ACE data, 1998. Note the abrupt change halfway through day 275 [11].

The magnitude of the magnetic field, velocity, proton density and Alfvén speed appear to have the most abrupt changes. Observe the shortness of the time interval over which the changes occur. Shocks are also caused by Corotating Interacting Regions discussed Section 1.6.

1.6 Corotating Interaction Regions

Following the Parker spiral, the magnetic field of the sun establishes a current sheet called the Heliospheric current sheet. With radial and lateral variance, the Heliospheric current sheet warps through the interplanetary medium and creates an interface between the low latitude slow wind and the high latitude fast wind [5]. The fast and slow wind approximately follow the Parker spiral producing regions of alternating fast and slow winds called Corotating Interaction Regions. In regions where the fast wind overtakes the slow wind, a shock can form, sometimes in two directions. The current sheet is less warped during solar minimum and has a shallow inclination angle to the equator. During solar maximum the inclination angle steepens and increases the interaction between the fast and slow wind.

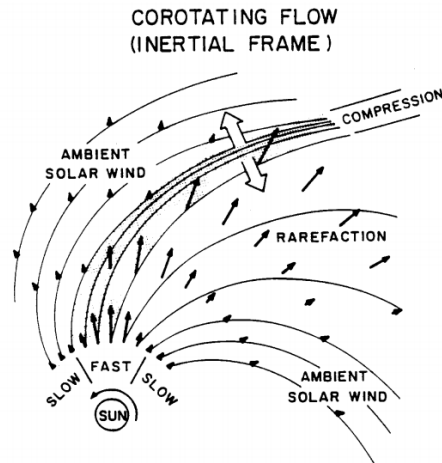


Figure 7: A Corotating interaction region aligning fast and slow winds in a current sheet [12].

When a fast wind outruns the slow wind, a rarefaction region forms of lower density and temperature than a compression region. A simplified picture is shown in Figure 6. The CIR's produce perturbations at earth and can accelerate particles to high energies.

Chapter 2

Magnetohydrodynamics

2.1 Background of MHD

The interaction of conducting fluids and magnetic fields drives much of the dynamics of the interstellar medium. Faraday's discovery of electromagnetic induction led to early advances in metallurgy and better methods of obtaining aluminum previously done via chemical processes [13]. In highly conducting fluids, magnetic flux is conserved and any time variation of flux establishes electrical currents that oppose the change in flux. The conducting fluid attempts to preserve the magnetic field structure, or freeze the flux from any relative movement of the two. In the interplanetary environment, the solar wind is the conducting fluid preserving the magnetic field structure of the sun dragging it out into its spiral shape with the rotation of the sun. Many interesting properties are observed with the application of Maxwell's equations to the Navier-Stokes equations.

Few practical applications of magnetohydrodynamics (MHD) were of interest to engineers until the abundance of plasmas and magnetic fields in the universe became apparent. The field advanced from the work of Hannes Alfvén who coined the term MHD in 1942 and discovered transverse propagations of magnetic field lines called Alfvén waves [13]. A fleet of satellites have made in situ measurements of the solar wind and interplanetary environment since 1960 discovering magnetohydrodynamic and turbulent processes affecting the evolution of the solar wind.

2.2 Equations of MHD

It is fitting to introduce the equations and conditions of MHD from basic principles with all equations in SI units outlined further in [13]. We start with the establishment of an electrical current with the generalized form of Ohm's law for a conductor moving in a rest frame

$$\vec{j} = \sigma(\vec{E} + \vec{u} \times \vec{B}) \quad (2)$$

where \vec{j} is the current density, \vec{E} is the electric field and $\vec{u} \times \vec{B}$ is the Lorentz force. The material dependent parameter σ is the conductivity whose value determines the degree to which magnetic flux is preserved in conducting media. Time invariant magnetic fields do not perform work on charged particles given by the Lorentz force in Eq. 3.

$$\vec{f} = q(\vec{E} + \vec{u} \times \vec{B}) \quad (3)$$

For conductors moving at nonrelativistic velocities, the electric field in Eq. 3 is dominated by $\vec{u} \times \vec{B}$. The solar wind is a low density conducting fluid and the force between individual charges is negligible and less significant than the bulk force on the medium. Rewriting Eq. 3 in the volumetric version and safely omitting \vec{E} we have

$$\vec{F} = \vec{j} \times \vec{B} \quad (4)$$

where the force \vec{F} is expressed in Nm^{-3} .

The remaining equations needed for MHD phenomena are obtained from Maxwell's equations. We start with the Ampere Maxwell law for the curl of the magnetic field

$$\vec{\nabla} \times \vec{B} = \mu \left(\vec{j} + \epsilon_0 \frac{\partial \vec{E}}{\partial t} \right) \quad (5)$$

where μ is the permeability of the conducting fluid and not that of free space as is the permittivity in the second term called the displacement current. We can rewrite the displacement current of the Ampere Maxwell law with current density and observe the scaling with conductivity in the denominator in Eq. 6.

$$\epsilon_0 \frac{\partial \vec{E}}{\partial t} \sim \frac{\epsilon_0 \partial \vec{j}}{\sigma \partial t} \ll \vec{j} \quad (6)$$

The conductivity of the solar wind diminishes the displacement current term thus for MHD we retain the pre-Maxwell form as the ampere law.

$$\vec{\nabla} \times \vec{B} = \mu \vec{j} \quad (7)$$

Taking the divergence of both sides of Eq. 7, the left hand side is identically zero. We arrive at a statement of divergence of the current density that is equal to zero.

$$\vec{\nabla} \cdot \vec{j} = 0 \quad (8)$$

This statement also comes immediately from local conservation of charge when the time rate of change of charge density is neglected.

We arrive at the last needed equation with Faraday's Law

$$\vec{\nabla} \times \vec{E} = -\frac{\partial \vec{B}}{\partial t} \quad (9)$$

where the absence of a second term found in the Ampere Maxwell law is due to the absence of magnetic monopoles. Taking the divergence of both sides as in Eq. 7 we arrive at the differential form of Gauss's law for magnetic fields, divergence free as it must.

$$\vec{\nabla} \cdot \vec{B} = 0 \quad (10)$$

Equations 2, 4, and 6-9 are the initial equations needed to investigate Alfvén waves, magnetic diffusivity and turbulence in the solar wind after an introduction to traditional turbulence in Chapter 3.

2.3 Alfvén Waves

The interplanetary medium is highly dynamic and presents magnetohydrodynamic and turbulent challenges from the corona to voyagers' current distances where interesting properties

are still being recorded. The interaction of the sun's rotating magnetic field and high conductivity of the turbulent solar wind alter the spectrum of velocity and magnetic field fluctuations. The physics of solar wind heating, mentioned in section 4.1, may be influenced by low frequency propagating waves called Alfvén waves. Their origin arises from Faraday's law of induction and is permitted by the high conductivity of the solar wind. We begin with the integral form of Faraday's law

$$\oint_C \vec{E} \circ d\vec{l} = -\frac{d}{dt} \int_S \vec{B} \circ d\vec{S} \quad (11)$$

that states that a circulating electric field of a closed contour results from time varying magnetic flux. Rewriting the left hand side using Ohm's law, retaining only the first term of Eq. 2 and inserting into Eq. 11 we have:

$$\frac{1}{\sigma} \oint_C \vec{j} \circ d\vec{l} = -\frac{d}{dt} \int_S \vec{B} \circ d\vec{S} \quad (12)$$

In the limit that $\sigma \rightarrow \infty$, the left hand side vanishes, thus the time rate of change of magnetic flux is zero.

$$\frac{d}{dt} \int_S \vec{B} \circ d\vec{S} = 0 \quad (13)$$

The statement of Eq. 13 has profound implication for the behavior of magnetic fields in highly conducting plasmas. The time rate of change of the magnetic field structure in nearly perfectly conducting plasmas is zero. This result describes the freezing of the sun's magnetic field by the solar wind that enhances the effect observed as the Parker spiral. An illustration is shown in Figure 6.

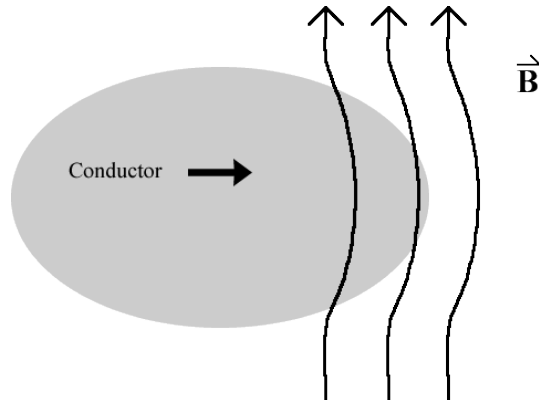


Figure 8: A conducting medium preserves a magnetic field. The field diffuses through the conductor.

A magnetic field cannot be imposed abruptly in a good conductor. The field requires a finite time to diffuse through the medium altered by the velocity and the conductivity of the conducting medium and the strength of the magnetic field [13]. We derive the diffusion equation by taking the curl of Ohm's law:

$$\frac{1}{\sigma}(\vec{\nabla} \times \vec{j}) = \vec{\nabla} \times \vec{E} + \vec{\nabla} \times (\vec{u} \times \vec{B}) \quad (14)$$

Solving Ampere's law, Eq. 7, for \vec{j} and inserting and replacing $\vec{\nabla} \times \vec{E}$ with the right hand side of Faraday's law, Eq. 9, we have:

$$\frac{1}{\mu\sigma} \vec{\nabla} \times (\vec{\nabla} \times \vec{B}) = -\frac{\partial \vec{B}}{\partial t} + \vec{\nabla} \times (\vec{u} \times \vec{B}) \quad (15)$$

Using the trig identity $\vec{\nabla} \times (\vec{\nabla} \times \vec{B}) = \vec{\nabla}(\vec{\nabla} \cdot \vec{B}) - \nabla^2 \vec{B}$ for the left hand side of (15) and noting that the divergence of the magnetic field is zero we arrive at the induction equation:

$$\frac{\partial \vec{B}}{\partial t} = \vec{\nabla} \times (\vec{u} \times \vec{B}) + \frac{1}{\mu\sigma} \nabla^2 \vec{B} \quad (16)$$

Letting $u \rightarrow 0$ the induction equation resembles the heat transfer equation and $(\mu\sigma)^{-1}$ is called the diffusivity with units m^2s^{-1} [2].

Consider a finite magnetic field depicted in Figure 6. As the conducting medium travels into the field, magnetic induction establishes electrical currents in the medium to oppose the change in magnetic flux. This occurs likewise when the medium exits the field. For highly conducting mediums travelling through magnetic fields, the bulk flow will experience magnetic drag as the field diffuses through the medium. The magnetic field also introduces damping effects similar to processes used in metallurgy to minimize movement of the fluid. The modification of the magnetic field experiences a restoring force analogous to tension on a string. This restoration results in the propagation of magnetohydrodynamic waves called Alfven waves. The derivation of an Alfven wave expression will be outlined for brevity and is more thoroughly developed in [13].

We begin with the induction equation and consider a uniform magnetic field \vec{B}_0 and perturb the system by infinitesimal changes to the velocity and magnetic field \vec{u} and \vec{B} , respectively. Substituting resulting perturbations of current density \vec{j} and magnetic field \vec{b} into Eq. 16 and 7 and implementing the Navier-Stokes equation (Chapter 3) we have:

$$\rho \frac{\partial \vec{u}}{\partial t} = (\vec{j} \times \vec{B}_0) - \vec{\nabla} p + \rho\nu \nabla^2 \vec{u} \quad (17)$$

Implementing the vorticity equation from fluid dynamics, eliminating \vec{j} and defining $\lambda \equiv (\mu\sigma)^{-1}$ we have:

$$\frac{\partial^2 \vec{\omega}}{\partial t^2} = \frac{1}{\rho\mu} (\vec{\nabla} \cdot \vec{B})^2 \vec{\omega} + (v + \lambda) \nabla^2 \left(\frac{\partial \vec{\omega}}{\partial t} \right) - \lambda v \nabla^4 \vec{\omega} \quad (18)$$

We can solve for ω by assuming a plane wave solution with $\omega_0 \exp [i(\vec{k} \cdot \vec{x} - 2\pi f t)]$ and wavenumber \vec{k} where k_{\parallel} is parallel to B_0 and we have:

$$2\pi f = -\left[\frac{(v+\lambda)k^2}{2} \right] i \pm \left[\frac{B_0^2 k_{\parallel}^2}{\rho\mu} - \frac{(v-\lambda)^2 k^4}{4} \right]^{\frac{1}{2}} \quad (19)$$

Considering an ideal fluid, we take ν and λ as zero and find

$$2\pi f = \pm \frac{B_0 k_{\parallel}}{\sqrt{\rho\mu}} \quad (20)$$

and define $v_a \equiv B_0/\sqrt{\rho\mu}$ as the speed of propagation of the transverse wave called an Alfvén wave that propagates along the magnetic field line parallel and antiparallel. The magnetic field acts as the restoring force similar to tension on a string depicted in Figure 9.

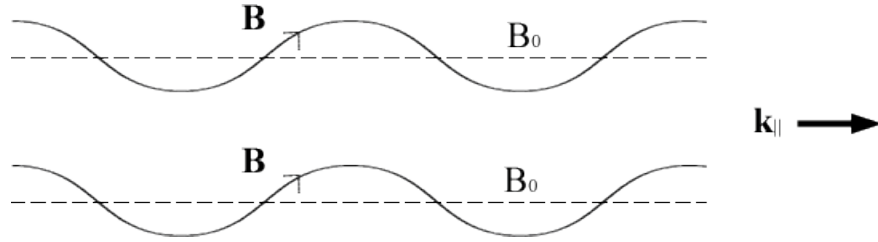


Figure 9: Alfvén waves resemble waves on a string.

Alfvén waves may largely contribute to solar wind turbulence and the origin of the solar wind itself. Magnetohydrodynamic waves are omitted by the sun from the interaction of the plasma and the sun's magnetic field. The high temperature of the corona may also be influenced by Alfvén waves and other magnetosonic waves that are longitudinal magnetohydrodynamic waves that propagate perpendicular to the magnetic field [5].

Chapter 3

Turbulence

3.1 Elements of Turbulence

Traditional turbulent processes demonstrate chaotic and stochastic changes in velocity, density and dissipation over varying length and energy scales. The non linear nature of turbulent flows occur in liquids, gases and plasmas and is most publicly known as sudden position changes in aircraft. Less known to the public is the difficulty turbulence presents for accurate weather forecasting. Stochastic dynamics are observed on scales as small as the interior of cells to stars and interplanetary plasmas. Some of the earliest descriptions of turbulence are detailed in drawings by Leonardo de Vinci, well before the development of Newtonian mechanics or sufficient mathematical framework to approach the nonlinear physics [14].

Turbulent physics advanced in the 19th century with the publication of the Navier-Stokes equations that model fluid flow in terms of velocity, rather than position, and solutions to the equations remain an important unsolved problem in physics and mathematics. Measurement of the fluctuation of solar wind velocity and magnetic data indicate that turbulent processes influence the behavior of the solar wind and interplanetary environment. Much evidence suggests that turbulence is central to the solar wind heating problem.

3.2 The Navier-Stokes Equation

Determinate systems, when provided identical initial conditions, will evolve in same manner. Perturbing the initial conditions, the evolution and outcome of the system retains information about the perturbation. In turbulent systems, perturbations of the initial conditions result in vastly different outcomes where information about the perturbation of initial conditions is lost. Turbulent systems are particularly sensitive to boundary and initial conditions. The analysis of nonlinear flows begins with a fluid form of Newton's second law as a nonlinear partial differential equation called the Navier-Stokes equation.

$$\frac{\partial \vec{u}}{\partial t} + \vec{u}(\vec{\nabla} \cdot \vec{u}) = \frac{1}{\rho} \vec{\nabla} P + \nu \nabla^2 \vec{u} \quad (21)$$

The velocity field is \vec{u} , the density and pressure are ρ and P , respectively, and ν is the kinematic viscosity [13]. A simplification of Eq. 21 is generally made for incompressible flows and the unfortunate language of the term makes it necessary to differentiate it from a fluid that is incompressible. In general, liquids are approximated as incompressible and gives rise to the continuity equation, thus the velocity field is divergence free. If the density changes little over large scales, as in the solar wind, it is sufficient to model the fluid as an incompressible flow and retain the divergence free velocity field. Thus the second term of the left hand side of Eq. 21 vanishes and the solar wind is taken as an incompressible flow, not an incompressible fluid.

Properties influencing turbulent flows are best developed from elementary treatments on turbulence with liquid flowing through a pipe. The boundary conditions of the pipe alter the flow of the liquid. The velocity of the flow is greatest at the center and is static at the surface of the pipe introducing shear stress in the flow shown in Figure 7.

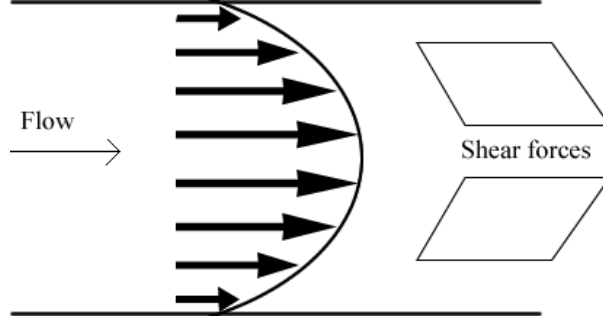


Figure 7: Fluid elements distort due to shear stress as fluid layers slide past each other at different rates.

For an ideal fluid without shear forces, the flow remains curl free. For fluids of low viscosity, surfaces can still influence significant forces due to shear stress leading to curl of the flow. These dynamics evolve producing the nonlinear behavior of turbulent flows.

The ratio of inertial forces to viscous forces determines the degree to which turbulence occurs where inertial forces arise from bulk motion of the fluid and viscous forces arise from gradients of shear forces. The ratio of inertial to viscous forces taken on a characteristic length scale is a dimensionless number called the Reynolds number and is defined in Eq. 22.

$$Re \equiv \frac{ul}{\nu} \quad (22)$$

The Reynolds number is generally large for most fluids and suggests turbulent flows where u is the velocity of the fluid, l is the characteristic length scale and ν is the kinematic viscosity. For increasingly small length scales the Reynolds number vanishes as expected from physical arguments where little room exists for nonlinearities to cascade [15]. For increasingly small values of velocity, motion collectively stops and turbulence cannot form in static systems. Various degrees of turbulent flows are shown in Figure 8.

For highly viscous flow with $Re \rightarrow 0$ we see in the top image of Figure 8 an ideal flow where surface influences and shear forces are negligible. For a Reynolds number of 100 the flow around a cylinder resembles the third image of Figure 3 where large scale eddies are evident. The fifth image of Figure 8 demonstrates fully developed turbulence with Reynolds number on the order of 10^6 . Low Reynolds numbers correspond to Laminar flow where little disruption occurs perpendicular to the velocity [15]. The transition from laminar flow to turbulent flow is often observed with the rising of cigarette smoke. The transition from laminar flow to turbulent flow is neither always clear nor sudden.

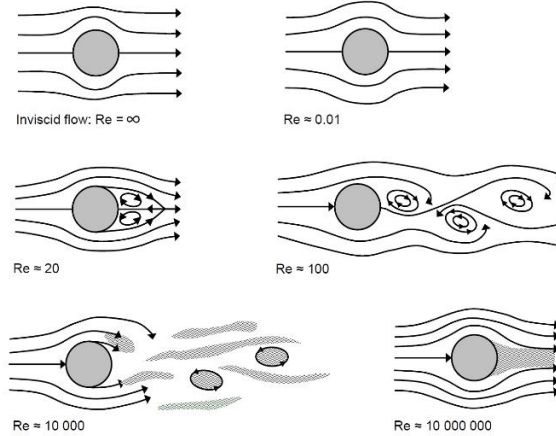


Figure 8: Turbulence relation to Reynolds number. $Re \ll 1$ is shown at the top with $Re \sim 10^6$ shown at the bottom [16].

The various stages and scales of turbulence provide difficulties in engineering practices aerodynamics, MHD and general fluid flows. Turbulence is present in the solar wind and fully developed turbulence undergoes cascades in energy and length scales that affect the evolution of the spectrum of the solar wind velocity and magnetic field fluctuations.

3.3 Kolmogorov Theory

Eddies of various size and energy scales are observed in turbulent systems. Large eddies break into medium scale eddies that break into small eddies. The cascade of turbulent flow from large to small scales is modeled by an energy spectrum in the form of a power law. The Kolmogorov theory, first published in 1942, is derivable from energy conservation and dimensional analysis [5]. There are three general scales that influence the solar wind evolution of which the Kolmogorov theory of our analysis relies on one. At the largest scales, the energy input from the sun is evident in the fluctuations and at the smallest scale eddies dissipate into heat. Our analysis focuses between the energy containing and dissipation scales called the inertial range and the general form of the Kolmogorov model is given by Eq. 23.

$$E(k) = C_K \varepsilon^{2/3} k^{-5/3} \quad (23)$$

The energy spectrum as a function of the wavenumber, $E(k)$ depends on the dimensionless parameter C_K , the energy cascade rate ε and the spectrum scale k with units of $length^{-1}$ [14]. The exponent value of k is determined through analysis of the velocity spectra. A simplified diagram of the energy cascade is shown in Figure 9.

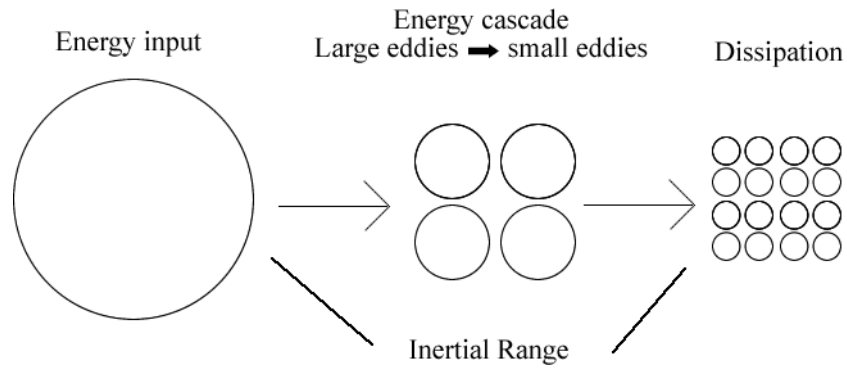


Figure 9: Large scale eddies cascade into small eddies that dissipate as heat. Between the energy containing and dissipation scales lies the inertial range.

The spectrum of velocity and magnetic field fluctuations provides information about the evolution of the solar wind. An example of the power law obtained through the spectrum of velocity or magnetic field fluctuations is shown in Figure 10.

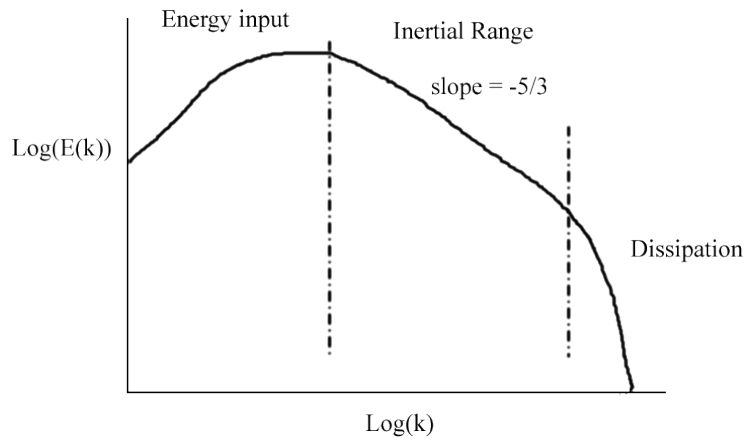


Figure 10: The power law predicted by Kolmogorov theory is $f^{-5/3}$ in the inertial range.

The sketched slope of figure 10 is the form of the velocity spectra expected and confirmed by previous studies. Variations of the $-5/3$ law are also observed and is the focus of Chapter 4 of the evolution of the spectrum of the velocity fluctuations.

Chapter 4

The Spectrum of Velocity Fluctuations

4.1 Motivation

The nonlinear behavior of turbulent systems remains an unsolved problem in mathematics and physics. Turbulence occurs in circulatory systems, rivers, wind flow, the core of the earth, the sun, the solar wind and generally everywhere fluid flows. Better understanding of turbulence evolution is necessary for advancements in aerospace engineering for safer travel, weather forecasting and predictions of solar events that result in geomagnetic storms. Turbulent processes that take place on the sun also occur in the solar wind. Many spacecraft make in situ measurements of the solar wind and establishes a turbulence laboratory covering many size, energy, and time scales. The measurement of solar wind variation with distance allows analysis that is compared to predictions of turbulence theories, particularly Kolmogorov theory.

The closest in situ measurements of the sun were made at .3 AU. Measurements closer are impractical with current technology and observation of turbulence in the solar wind is the next best means of studying turbulent processes that occur in the sun. Large solar flares or CME's can damage satellite hardware and induce high currents in electrical power grids. Solar flares and CME's are not yet predictable but are anticipated more during solar maximum. Several Apollo missions narrowly avoided large solar flares that may have been catastrophic to the mission.

The temperature profile of the solar wind does not follow that of an adiabatic expansion as predicted by thermodynamics. The solar wind temperature remains higher than expected thus a source is by some means heating the solar wind. Evidence strongly indicates that turbulence is a primary source of the solar wind heating and is likely to affect the high temperature of the sun's corona. Many advances in physics can result from a better understanding of turbulent processes that are of equal importance in engineering and technological applications.

4.2 Overview

Voyager II launched on August 20, 1977 and passed Jupiter two years later. The data set is merged from plasma and magnetic field measurements and from this we obtain the needed data. We developed a data preprocessing routine to extract user defined intervals and mark the data with invalid flags for time gaps and invalid data. The processed file contains header information interpreted by the Fast Fourier Transform (FFT) routines that produce the power spectral density plots. From this we obtain the slope that corresponds to the power law of Eq. 23.

4.3 Data Preprocessing

An ideal data set consists of samples taken at regular intervals. The Voyager II merged data set contains timing gaps and timing changes. These unavoidable data irregularities are added to missing and invalid data that must be marked as unusable before FFT analysis begins. We developed a bad-point-editing routine to first extract a specified time interval from the data set

and determine where missing data exists. Often gaps are visible by viewing the unprocessed data set by noting jumps in the time sequence. The bad-point routine computes the number of data rows missing based on the standard interval timing and fills each row entirely with a preset bad-point value of -999.9.

The data set contains previously marked invalid data and sporadic impossibly large values evident from Figure 11. Any row containing invalid velocity data is flagged bad with -999.9 and is bypassed by the FFT routines.

233.75895,	1.3338920e+008,	-68225798.,	1288019.5,	4.44000,	-2.32000,	3.12000,	2.15000,	402.300,	-40:
233.76006,	1.3339005e+008,	-68223716.,	1288206.1,	4.46000,	-1.90000,	3.27000,	2.36000,	405.300,	-40:
233.80451,	1.3342412e+008,	-68136137.,	1295678.4,	4.46000,	-1.90000,	3.27000,	2.37000,	395.300,	-39:
233.80562,	1.3342497e+008,	-68136137.,	1295865.5,	4.14000,	-2.42000,	0.756000,	3.27000,	397.600,	-39:
233.80673,	1.3342582e+008,	-68136137.,	1296052.6,	4.38000,	-3.16000,	1.39000,	2.82000,	392.300,	-39:
233.80784,	1.3342668e+008,	-68134048.,	1296239.,	4.38000,	-3.16000,	1.62000,	2.57000,	389.500,	-38:
233.80895,	1.3342753e+008,	-68131960.,	1296465.9,	4.43000,	-3.17000,	2.09000,	2.28000,	389.400,	-38:
233.81006,	1.3342838e+008,	-68129870.,	-99999.9,	-4.25000e+037,	-4.25000e+037,	4.25000e+037,	83.0000,	12966.	-38:
233.81118,	1.3342924e+008,	-68127781.,	1296801.2,	4.35000,	-3.16000,	2.66000,	389.700,	389.700,	-38:
233.81229,	1.3343009e+008,	-68125692.,	1296988.3,	4.38000,	-3.16000,	2.36000,	388.000,	388.000,	-38:

Figure 11: A sample of data integrity problems from the merged Voyager II data set. Gaps are visible with “timing changes.” Visible are the pre-marked “missing data” and impossibly large “invalid data.”

After timing changes, missing, and invalid data rows are flagged or filled with the bad-point value, the routine computes averages and standard deviations of the needed data. A final sweep of the data flags any row as bad if any value exceeds three standard deviations of the mean. This ensures data integrity for the final FFT processing.

4.4 Velocity Spectra

The spectra of the velocity and magnetic field fluctuations of the solar wind are expected to be similar as turbulent eddies cascade down in energy and scale. Previous studies, particularly Roberts 2010 [17], indicate that the power law relationship is closer to $f^{-3/2}$ in the inertial range. The spectra in Figure 12 from Bruno and Carbone, 2005 [18], show several slopes of magnetic field fluctuations between .3 and 1 AU using Helios data. The velocity spectra is expected to produce similar results. A signature of turbulence is a range of length and energy scales indicated by the various slopes. We initially extracted 10 day intervals from the Voyager II merged data set with 96 second resolution between 1 and 5 AU. The slopes of the spectra correlate little with the Kolmogorov -5/3 theoretical value or the -3/2 obtained by spectra from other spacecraft data sets.

Figure 13 shows an overlay of spectra at approximately 3 AU demonstrating a sample of the variation in velocity spectra power law. The variance of slopes obtained makes averages an inaccurate representation of the solar wind turbulence. The 10 day intervals extracted had an average of 55 percent usable data after preprocessing. We adapted interval extraction to avoid significant timing changes in the data set described in section 4.5

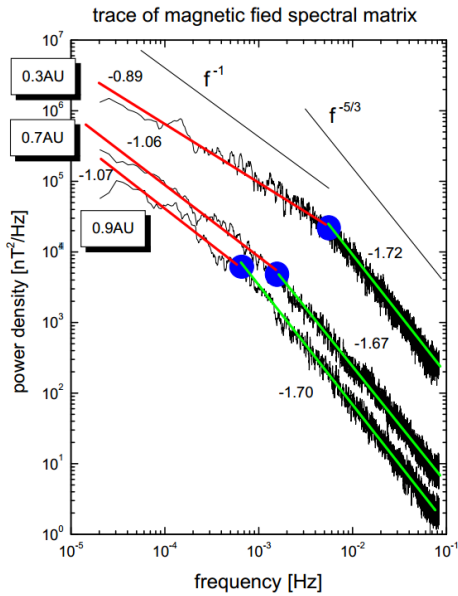


Figure 12: PSD plot between .3 and .9 AU. Bruno and Carbone, 2005 [18].

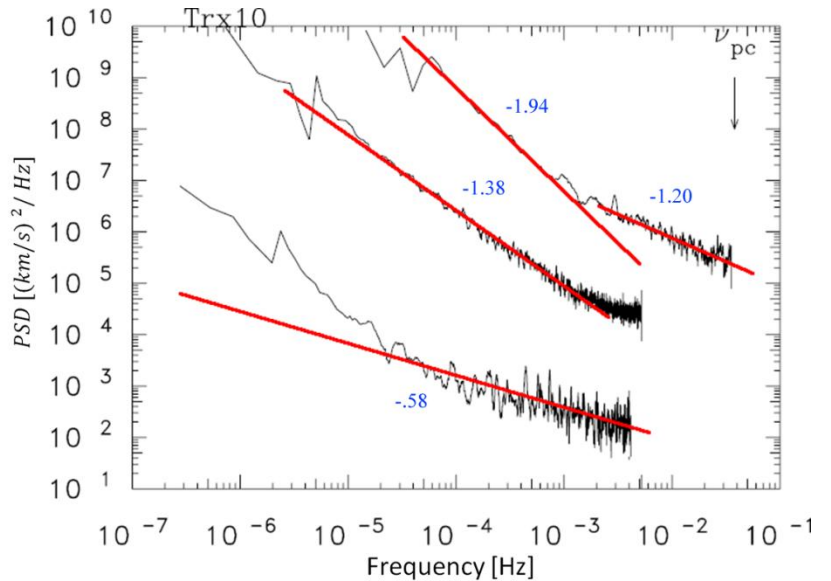


Figure 13: Slopes of the power spectra vary significantly and may not accurately reflect the turbulent processes.

4.5 Interval Modification

Unmarked time gaps in the data set span from 3 minutes to more than a day of missing data. We modified the preprocessing routine to output time gap data permitting us to choose intervals between time gaps. Figure 14 shows an interval with significant data loss indicated by the rows of bad-point flags added.

```

The following are days in which the voyager data files change time intervals.
Total number of delta changes: 68

Start row: 6668
End row: 11124

From: day 91, hour 0
To: day 99, hour 0

There were 60 invalid data points and 20 missing data points.
Each has been flagged to bad_flag_value.
Of 4457 rows of data, 2742 rows have been added, flagged to bad_flag_value

```

Day	Hour	Decimal of the day	Value at change	Row #	Delta	Rows added
91	00	0.00121	91.00121	6669	0.00222	1
91	00	0.02676	91.02676	6691	0.00222	1
91	00	0.03010	91.03010	6692	0.00333	2
91	01	0.05010	91.05010	6709	0.00222	1
91	05	0.21565	91.21565	6735	0.13778	123
91	06	0.27343	91.27343	6786	0.00222	1
91	14	0.61898	91.61898	7094	0.00444	3
92	05	0.21232	92.21232	7508	0.13444	120
92	07	0.32121	92.32121	7605	0.00222	1
92	08	0.36121	92.36121	7638	0.00444	3

Figure 14: Data intervals with little usable data occur frequently.

We extract the largest interval possible between time gaps and reproduce the PSD plots. This method increases the usable data to an average of 93 percent. The velocity spectra show similar variance exemplified in Figure 13 obtained by extracting intervals of equal length in succession.

4.6 Summary

Observing the evolution of the spectrum of the solar wind velocity fluctuations provides details of how turbulent processes change in time. The $-5/3$ law of Kolmogorov turbulence theory is well observed in various fluid flows. The deviation from the $-5/3$ law is observed in the transient solar wind as radial distance increases. The PSD plots generated initially were successive 10 day plots and later modified to 5 hour plots. The slopes of the spectra obtained did not converge to reasonable results obtained by analyses from other spacecraft. We measured the power law of intervals as short as 6 hours and partitioned the slopes by the fifth of an AU and find that slopes are not converging to expected values. Slopes obtained from the Voyager II data vary quickly from as low as $-.5$ to as high as -2 . After exhausting the data set we suspect the accuracy of the voyager data and begin surveying data from Voyager I. Observing the deviation of the power law from the $-5/3$ theoretical value is important in turbulence research and we continue research with the less studied velocity fluctuations of the solar wind.

References

- [1] Gleick, James. *Isaac Newton*. New York: Pantheon, 2003. Print.
- [2] Kivelson, M. G., and C. T. Russell. *Introduction to Space Physics*. Cambridge: Cambridge UP, 1995. Print.
- [3] Hesperides. *Biographical Memoirs - National Academy Of Sciences*. Vol. XXv. N.p.: Hesperides, 2007. Print.
- [4]
- [5] Meyer-Vernet, Nicole. *Basics of the Solar Wind*. Cambridge, UK: Cambridge UP, 2007. Print.
- [6] Image source: <http://ham.space.umn.edu/cattell/PHYS4611/lecture%5oct.pdf>
- [7] Freeman, John W. *Storms in Space*. Cambridge, UK: Cambridge UP, 2001. Print.
- [8] Dynamics of the Interplanetary Gas and Magnetic Fields. *Astrophys. J.*, Vol. 128 (November 1958), doi:10.1086/146579 by E. N. Parker
- [9] Howard, Timothy. *Coronal Mass Ejections: An Introduction*. New York: Springer, 2011. Print.
- [10] Image source: <http://sohowww.nascom.nasa.gov/gallery/bestofsoho.ht>
- [11] <http://www.srl.caltech.edu/ACE/ASC/DATA/level3/mag/magswesummary.cgi?LATES T=1>
- [12] Pizzo, V. J., and J. T. Gosling. "Formation and Evolution of Corotating Interaction Regions and Their Three Dimensional Structure." *Space Science Reviews* 89.1-2 (1999): 21-52. Web.
- [13] Davidson, P. A. *An Introduction to Magnetohydrodynamics*. Cambridge: Cambridge UP, 2001. Print.
- [14] Frisch, U., and A. N. Kolmogorov. *Turbulence: The Legacy of A.N. Kolmogorov*. Cambridge [England: Cambridge UP, 1995. Print.
- [15] Mathieu, Jean, and Julian Scott. *An Introduction to Turbulent Flow*. Cambridge: Cambridge UP, 2000. Print.
- [16] Image source: <http://cronodon.com/BioTech/Biorheology.html>

- [17] Roberts, D. A. (2010), Evolution of the spectrum of solar wind velocity fluctuations from 0.3 to 5 AU, *J. Geophys. Res.*, 115, A12101, doi:10.1029/2009JA015120
- [18] Roberto Bruno and Vincenzo Carbone, "The Solar Wind as a Turbulence Laboratory", *Living Rev. Solar Phys.*, 2, (2005), 4. [Online Article]: cited [jdate], <http://www.livingreviews.org/lrsp-2005-4>